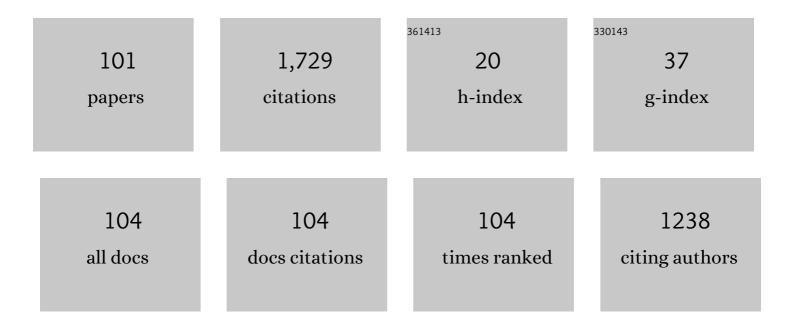
List of Publications by Year in descending order

Source: https://exaly.com/author-pdf/7840379/publications.pdf Version: 2024-02-01



#	Article	IF	CITATIONS
1	Abnormal growth of faceted (WC) grains in a (Co) liquid matrix. Metallurgical and Materials Transactions A: Physical Metallurgy and Materials Science, 1996, 27, 2809-2819.	2.2	232
2	Effect of Interface Structure on the Microstructural Evolution of Ceramics. Journal of the American Ceramic Society, 2006, 89, 2369-2380.	3.8	132
3	Grain boundary faceting and abnormal grain growth in nickel. Metallurgical and Materials Transactions A: Physical Metallurgy and Materials Science, 2000, 31, 985-994.	2.2	103
4	Vacancy defects and the formation of local haeckelite structures in graphene from tight-binding molecular dynamics. Physical Review B, 2006, 74, .	3.2	81
5	Charged clusters in thin film growth. International Materials Reviews, 2004, 49, 171-190.	19.3	68
6	Reconstruction and evaporation at graphene nanoribbon edges. Physical Review B, 2010, 81, .	3.2	55
7	Effect of the Liquidâ€Forming Additive Content on the Kinetics of Abnormal Grain Growth in Alumina. Journal of the American Ceramic Society, 2003, 86, 1421-1423.	3.8	54
8	Charged nanoparticles in thin film and nanostructure growth by chemical vapour deposition. Journal Physics D: Applied Physics, 2010, 43, 483001.	2.8	52
9	The formation of pentagon-heptagon pair defect by the reconstruction of vacancy defects in carbon nanotube. Applied Physics Letters, 2008, 92, 043104.	3.3	33
10	Formation of carbon nanotube semiconductor-metal intramolecular junctions by self-assembly of vacancy defects. Physical Review B, 2007, 76, .	3.2	32
11	Formation and development of dislocation in graphene. Applied Physics Letters, 2013, 102, .	3.3	31
12	Generation of charged nanoparticles during the synthesis of carbon nanotubes by chemical vapor deposition. Carbon, 2009, 47, 2511-2518.	10.3	30
13	Gas phase generation of diamond nanoparticles in the hot filament chemical vapor deposition reactor. Carbon, 2016, 106, 289-294.	10.3	30
14	Generation of Charged Nanoparticles during Synthesis of ZnO Nanowires by Carbothermal Reduction. Aerosol Science and Technology, 2009, 43, 120-125.	3.1	26
15	Spontaneous generation of negatively charged clusters and their deposition as crystalline films during hot-wire silicon chemical vapor deposition. Pure and Applied Chemistry, 2006, 78, 1715-1722.	1.9	25
16	Comparison of the Deposition Behavior of Charged Silicon Nanoparticles between Floating and Grounded Substrates. Journal of Physical Chemistry C, 2014, 118, 11946-11953.	3.1	25
17	Effect of Grain Coalescence on the Abnormal Grain Growth of Pb(Mg _{1/3} Nb _{2/3})O ₃ â€35 mol% PbTiO ₃ Ceramics. Journal of the American Ceramic Society, 2002, 85, 965-968.	3.8	24
18	Pore–Boundary Separation Behavior during Sintering of Pure and Bi ₂ O ₃ â€Doped ZnO Ceramics. Journal of the American Ceramic Society, 2001, 84, 1398-1400.	3.8	21

#	Article	IF	CITATIONS
19	Generation of negative-charge carriers in the gas phase and their contribution to the growth of carbon nanotubes during hot-filament chemical vapor deposition. Carbon, 2008, 46, 1588-1592.	10.3	21
20	Generation of Charged Nanoparticles During the Synthesis of Silicon Nanowires by Chemical Vapor Deposition. Journal of Physical Chemistry C, 2010, 114, 3390-3395.	3.1	21
21	Effect of Electric Bias on the Deposition Behavior of ZnO Nanostructures in the Chemical Vapor Deposition Process. Journal of Physical Chemistry C, 2015, 119, 25047-25052.	3.1	20
22	Effect of Pulsed Electric Current on TRIP-Aided Steel. International Journal of Precision Engineering and Manufacturing - Green Technology, 2019, 6, 315-327.	4.9	18
23	Abnormal Grain Growth Occurring at the Surface of a Sintered BaTiO ₃ Specimen. Journal of the American Ceramic Society, 2004, 87, 1779-1781.	3.8	16
24	Equilibrium shape of nickel crystal. Philosophical Magazine, 2009, 89, 2989-2999.	1.6	16
25	Comparison of the Advantages Conferred by Mobility and Energy of the Grain Boundary in Inducing Abnormal Grain Growth Using Monte Carlo Simulations. Materials Transactions, 2009, 50, 2521-2525.	1.2	16
26	Generation of charged nanoparticles and their deposition during the synthesis of silicon thin films by chemical vapor deposition. Journal of Applied Physics, 2010, 108, 014313.	2.5	16
27	Reduction of amorphous incubation layer by HCl addition during deposition of microcrystalline silicon by hot-wire chemical vapor deposition. Solar Energy Materials and Solar Cells, 2011, 95, 211-214.	6.2	16
28	The role of pentagon–heptagon pair defect in carbon nanotube: The center of vacancy reconstruction. Applied Physics Letters, 2010, 97, 093106.	3.3	15
29	Non-classical crystallization of silicon thin films during hot wire chemical vapor deposition. Journal of Crystal Growth, 2017, 458, 8-15.	1.5	15
30	Comparison of Plasma Effect on Dewetting Kinetics of Sn Films Between Grounded and Floating Substrates. Electronic Materials Letters, 2020, 16, 72-80.	2.2	15
31	Grain boundary faceting and abnormal grain growth in nickel. Metallurgical and Materials Transactions A: Physical Metallurgy and Materials Science, 2000, 31, 985-994.	2.2	14
32	First-principles study of the effect of charge on the stability of a diamond nanocluster surface. Physical Review B, 2004, 69, .	3.2	14
33	Ex Situ Observation of Microstructure Evolution During Abnormal Grain Growth in Aluminum Alloy. Metallurgical and Materials Transactions A: Physical Metallurgy and Materials Science, 2012, 43, 5218-5223.	2.2	14
34	Synthesis of nanostructures using charged nanoparticles spontaneously generated in the gas phase during chemical vapor deposition. Journal Physics D: Applied Physics, 2018, 51, 463002.	2.8	14
35	Effect of Bias Applied to the Substrate on the Low Temperature Growth of Silicon Epitaxial Films during RF-PECVD. Crystal Growth and Design, 2018, 18, 5816-5823.	3.0	14
36	Plasma Etching Behavior of YOF Coating Deposited by Suspension Plasma Spraying in Inductively Coupled CHF3/Ar Plasma. Coatings, 2020, 10, 1023.	2.6	13

#	Article	IF	CITATIONS
37	Generation of Charged Nanoparticles During the Synthesis of GaN Nanostructures by Atmospheric-Pressure Chemical Vapor Deposition. Aerosol Science and Technology, 2012, 46, 1100-1108.	3.1	12
38	In-SituMeasurements of Charged Nanoparticles Generated During Hot Wire Chemical Vapor Deposition of Silicon Using Particle Beam Mass Spectrometer. Aerosol Science and Technology, 2013, 47, 46-51.	3.1	11
39	Effect of substrate bias on deposition behaviour of charged silicon nanoparticles in ICP-CVD process. Journal Physics D: Applied Physics, 2017, 50, 035201.	2.8	11
40	Coarsening Process of Penetrationâ€Twinned Grains in PMNâ€35 mol% PT Ceramics. Journal of the American Ceramic Society, 2004, 87, 125-128.	3.8	10
41	Three-dimensional simulation of microstructure evolution in damascene interconnects: Effect of overburden thickness. Journal of Electronic Materials, 2005, 34, 559-563.	2.2	10
42	Parallel three-dimensional Monte Carlo simulations for effects of precipitates and sub-boundaries on abnormal grain growth of Goss grains in Fe–3%Si steel. Philosophical Magazine, 2013, 93, 4198-4212.	1.6	10
43	Low temperature deposition of polycrystalline silicon thin films on a flexible polymer substrate by hot wire chemical vapor deposition. Journal of Crystal Growth, 2016, 453, 151-157.	1.5	10
44	Computer Simulation of Temperature Parameter for Diamond Formation by Using Hot-Filament Chemical Vapor Deposition. Coatings, 2018, 8, 15.	2.6	10
45	Generation of Charged SiC Nanoparticles During HWCVD Process. Electronic Materials Letters, 2020, 16, 498-505.	2.2	10
46	Yttrium Oxyfluoride Coatings Deposited by Suspension Plasma Spraying Using Coaxial Feeding. Coatings, 2020, 10, 481.	2.6	10
47	Abnormal Grain Growth of Pb(Mg _{1/3} Nb _{2/3})O ₃ â€35 mol% PbTiO ₃ Ceramics Induced by the Penetration Twin. Journal of the American Ceramic Society, 2002, 85, 3076-3080.	3.8	9
48	Various Allotropes of Diamond Nanoparticles Generated in the Gas Phase during Hot Filament Chemical Vapor Deposition. Nanomaterials, 2020, 10, 2504.	4.1	9
49	Effect of substrate materials in the low-pressure synthesis of diamond: approach by theory of charged clusters. International Journal of Materials Research, 2005, 96, 225-232.	0.8	9
50	Effect of grain boundary energy on surface-energy induced abnormal grain growth in columnar-grained film. Metals and Materials International, 2002, 8, 1-5.	3.4	8
51	Abnormal Grain Growth of Lead Zirconium Titanate (PZT) Ceramics Induced by the Penetration Twin. Journal of the American Ceramic Society, 2006, 89, 1530-1533.	3.8	8
52	Deformation Feature of Goss Grains in Fe-3%Si Steel Focused on Stored Energy after Cold Rolling. Materials Transactions, 2010, 51, 1547-1552.	1.2	8
53	Nonclassical Crystallization in Low-Temperature Deposition of Crystalline Silicon by Hot-Wire Chemical Vapor Deposition. Crystal Growth and Design, 2014, 14, 6239-6247.	3.0	8
54	Control of nanoparticle size and amount by using the mesh grid and applying DC-bias to the substrate in silane ICP-CVD process. Journal of Nanoparticle Research, 2017, 19, 1.	1.9	8

#	Article	IF	CITATIONS
55	Preparation of Highly (002) Oriented Ti Films on a Floating Si (100) Substrate by RF Magnetron Sputtering. Electronic Materials Letters, 2020, 16, 14-21.	2.2	8
56	Comparison of diamond nanoparticles captured on the floating and grounded membranes in the hot filament chemical vapor deposition process. RSC Advances, 2021, 11, 5651-5657.	3.6	8
57	Effect of SiO2 and TiO2 Addition on the Morphology of Abnormally Grown Large Pb(Mg1/3Nb2/3)O3-35 mol% PbTiO3 Grains. Journal of the American Ceramic Society, 2005, 88, 1992-1994.	3.8	7
58	Generation of Charged Nanoparticles and Their Deposition Behavior under Alternating Electric Bias during Chemical Vapor Deposition of Silicon. Journal of Physical Chemistry C, 2012, 116, 25157-25163.	3.1	7
59	Effect of the Carrier Gas Flow Rate on the Microstructure Evolution and the Generation of the Charged Nanoparticles During Silicon Chemical Vapor Deposition. Journal of Nanoscience and Nanotechnology, 2013, 13, 7127-7130.	0.9	7
60	Simultaneous increase in strength and ductility by decreasing interface energy between Zn and Al phases in cast Al-Zn-Cu alloy. Scientific Reports, 2017, 7, 12195.	3.3	7
61	Generation of Charged Ti Nanoparticles and Their Deposition Behavior with a Substrate Bias during RF Magnetron Sputtering. Coatings, 2020, 10, 443.	2.6	7
62	Effect of Bipolar Charging of SiH4 on the Growth Rate and Crystallinity of Silicon Films Grown in the Atmospheric Pressure Chemical Vapor Deposition Process. Electronic Materials Letters, 2020, 16, 385-395.	2.2	7
63	Effect of the Initial Structure on the Electrical Property of Crystalline Silicon Films Deposited on Glass by Hot-Wire Chemical Vapor Deposition. Journal of Nanoscience and Nanotechnology, 2012, 12, 5947-5951.	0.9	6
64	New understanding of the role of coincidence site lattice boundaries in abnormal grain growth of aluminium alloy. Philosophical Magazine Letters, 2015, 95, 220-228.	1.2	6
65	Effects of radio frequency power and gas ratio on barrier properties of SiOxNy films deposited by inductively coupled plasma chemical vapor deposition. Thin Solid Films, 2019, 669, 108-113.	1.8	6
66	Ex-Situ Time Sequential Observation on Island and Peninsular Grains in Abnormally Growing Goss Grains in Fe–3%Si Steel. Metals and Materials International, 2020, 26, 1200-1206.	3.4	6
67	Dependence of the Generation Behavior of Charged Nanoparticles and Ag Film Growth on Sputtering Power during DC Magnetron Sputtering. Electronic Materials Letters, 2021, 17, 172-180.	2.2	6
68	Effect of Pressure on the Film Deposition during RF Magnetron Sputtering Considering Charged Nanoparticles. Coatings, 2021, 11, 132.	2.6	6
69	Irregular or Smooth Grain Boundaries Evolved after Secondary Recyrstallization of Fe–3%Si Steel. Materials Transactions, 2012, 53, 658-661.	1.2	5
70	Formation of Tetrapod-Shaped Nanowires in the Gas Phase During the Synthesis of ZnO Nanostructures by Carbothermal Reduction. Journal of Nanoscience and Nanotechnology, 2013, 13, 7198-7201.	0.9	5
71	Effect of Asymmetric Hot Rolling on the Texture Evolution of Fe–3%Si Steel. Metals and Materials International, 2018, 24, 1369-1375.	3.4	5
72	Deposition Behavior of Boron-Doped Diamond with Varying Amount of Acetone by Hot Filament Chemical Vapor Deposition. Electronic Materials Letters, 2019, 15, 630-638.	2.2	5

#	Article	IF	CITATIONS
73	Unusual Dependence of the Diamond Growth Rate on the Methane Concentration in the Hot Filament Chemical Vapor Deposition Process. Materials, 2021, 14, 426.	2.9	5
74	Reply to the Comment on "Effect of Interface Structure on the Microstructural Evolution of Ceramics". Journal of the American Ceramic Society, 2007, 90, 2293-2295.	3.8	4
75	Effect of HCl addition on the properties of p-type silicon thin films during hot-wire chemical vapor deposition. Renewable Energy, 2013, 54, 85-90.	8.9	4
76	Alignment of nanoparticles, nanorods, and nanowires during chemical vapor deposition of silicon. Applied Physics A: Materials Science and Processing, 2015, 120, 889-895.	2.3	4
77	Misorientation Characteristics at the Growth Front of Abnormally-Growing Goss Grains in Fe–3%Si Steel. Metals and Materials International, 2021, 27, 5114-5120.	3.4	4
78	The Effect of Charged Ag Nanoparticles on Thin Film Growth during DC Magnetron Sputtering. Coatings, 2020, 10, 736.	2.6	4
79	Charging Effects on the Adsorption and Diffusion of Au Adatoms on MgO(100). Journal of the Physical Society of Japan, 2021, 90, 034602.	1.6	4
80	Ab-initio study of the effects of charging on the adsorption and diffusion of Au2 on MgO(100). Current Applied Physics, 2021, 24, 39-45.	2.4	4
81	Non-classical Crystallization of Bulk Crystals in Solution and of Thin Films in the Gas Phase by Chemical Vapor Deposition. Electronic Materials Letters, 2022, 18, 1-26.	2.2	4
82	Nonclassical Crystallization of an Al ₂ O ₃ Film by Positively Charged Secondary Nanoparticles during Aerosol Deposition. Crystal Growth and Design, 2021, 21, 7240-7246.	3.0	4
83	Structural and optical properties of H2 diluted c-Si/a-SiO x core-shell silicon nanowire. Applied Physics A: Materials Science and Processing, 2015, 118, 269-274.	2.3	3
84	Effect of the Dispersion State in Y5O4F7 Suspension on YOF Coating Deposited by Suspension Plasma Spray. Coatings, 2021, 11, 831.	2.6	3
85	Insulation Coating of Fe–Si–Cr Soft Magnetic Powder by Selective Oxidation. Metals and Materials International, 2022, 28, 1778-1782.	3.4	3
86	Beyond‑carbon-solvency effects of catalytic metal Ni on diamond growth. Diamond and Related Materials, 2020, 107, 107875.	3.9	3
87	Effect of the substrate bias in diamond deposition during hot filament chemical vapor deposition: Approach by non-classical crystallizationÂ. Advanced Materials Letters, 2018, 9, 638-642.	0.6	3
88	Generation of positively charged nanoparticles by fracto-emission and their deposition into films during aerosol deposition. Applied Surface Science, 2022, 593, 153466.	6.1	3
89	Misorientation characteristics of penetrating morphologies at the growth front of abnormally growing grains in aluminum alloy. Philosophical Magazine Letters, 0, , 1-8.	1.2	2
90	Abnormal grain growth in the nanostructured Invar alloy fabricated by electrodeposition. Philosophical Magazine Letters, 2012, 92, 589-596.	1.2	2

#	Article	IF	CITATIONS
91	Effects of the Size of Charged Nanoparticles on the Crystallinity of SiC Films Prepared by Hot Wire Chemical Vapor Deposition. Coatings, 2020, 10, 726.	2.6	2
92	Importance of Interfacial Structures in the Catalytic Effect of Transition Metals on Diamond Growth. ACS Omega, 2021, 6, 28432-28440.	3.5	2
93	Effect of Cooling Rate on Phase Transformation Behavior during Isothermal Annealing of SCr420 Steel. Steel Research International, 0, , 2100711.	1.8	2
94	Yttrium Oxyfluoride Coating Deposited with a Y5O4F7/YF3 Suspension by Suspension Plasma Spraying Under Atmospheric Pressure. Journal of Thermal Spray Technology, 0, , 1.	3.1	2
95	Formation of Pentagonal Dimples in Icosahedral Diamond Crystals Grown by Hot Filament Chemical Vapor Deposition: Approach by Non-Classical Crystallization. Coatings, 2019, 9, 269.	2.6	1
96	Phonon spectra of clean and Ni-terminated diamond (111) surfaces: An ab-initio study. Current Applied Physics, 2021, 21, 134-139.	2.4	1
97	Two-Step Deposition of Silicon Oxide Films Using the Gas Phase Generation of Nanoparticles in the Chemical Vapor Deposition Process. Coatings, 2021, 11, 365.	2.6	1
98	Effects of Sputtering Power, Working Pressure, and Electric Bias on the Deposition Behavior of Ag Films during DC Magnetron Sputtering Considering the Generation of Charged Flux. Electronic Materials Letters, 2022, 18, 57-68.	2.2	1
99	Effects of Electrostatic Interaction on the Formation of a Particle Depletion Zone by Charged Nanoparticles during the Chemical Vapor Deposition of Si Processes. Crystal Growth and Design, 2022, 22, 2490-2498.	3.0	1
100	Characteristics of Liquid Penetration into Undoped and Magnesiaâ€Doped Alumina. Journal of the American Ceramic Society, 2003, 86, 2206-2208.	3.8	0
101	Fabrication of Highly Transparent and Costâ€Effective Soda Lime Glass with Antireflective Nanostructures Using Silver Ink. Physica Status Solidi (A) Applications and Materials Science, 2018, 215, 1770-40	1.8	Ο